MODELING OF MICROWAVE RING RESONATORS USING THE FINITE-DIFFERENCE TIME-DOMAIN METHOD (FDTD)

Elena Semouchkina,[1] Wenwu Cao,[1,2] and Raj Mittra[3]
[1] Materials Research Laboratory
The Pennsylvania State University
University Park, Pennsylvania 16802
[2] Department of Mathematics
The Pennsylvania State University
University Park, Pennsylvania 16802
[3] Department of Electrical Engineering
The Pennsylvania State University
University Park, Pennsylvania 16802

Received 29 September 1999

ABSTRACT: *Scattering parameters of microstrip ring resonators (with and without slits) that are either edge or side coupled to the feedlines are simulated by the FDTD method. The strip conductors on the device can either be infinitely thin or finite in thickness. The simulations predict the occurrence of resonance peak splitting due to the simultaneous existence of magnetic and electric field coupling mechanisms. Excellent agreement was obtained between the simulation results and the measured data for a ring resonator. We have also shown that it is possible to use finite-difference time-domain simulations to determine the dielectric constant of substrate materials.* © 2000 John Wiley & Sons, Inc. Microwave Opt Technol Lett 24: 392–396, 2000.

Key words: *microstrip ring; microwave resonator; finite-difference time-domain method; scattering parameters; dielectric constant measurements*

1. INTRODUCTION

Microstrip ring resonator circuits are used in many microwave devices, including oscillators, filters, couplers, mixers, and antennas. They are also frequently utilized as test vehicles for material property characterization, particularly for the determination of the dielectric constant of thin-film substrates at microwave frequencies. The characterization method is based on the relationship between the resonance frequency and the so-called effective dielectric constant [1, 2]. The dielectric constant of the material is determined from the knowledge of the effective dielectric constant using approximate closed-form expressions that are derived by analyzing microstrip lines using the conformal mapping technique in the context of the quasi-TEM approximation [3–6]. These expressions have limited validity; therefore, attempts have been made to develop more sophisticated field analyses to describe the microwave performance of ring resonators, and improved accuracy has been obtained [7–11]. Nonetheless, problems still persist in some of these improved models: the "magnetic wall model" [8] does not account for the fringing fields; the "planar waveguide model" [9] uses an artificial assumption of a frequency-dependent width for parallel conducting plates. The more rigorous solution based on the variational principle and the "reaction concept" of electromagnetic theory [10] fails to include the higher order modes. The transmission-line analysis [11], on the other hand, makes a number of assumptions, which are not valid when the circuit model does not accurately represent the ring and coupling gap of the resonator.

Contract grant sponsor: Center for Dielectric Studies, Pennsylvania State University

In this paper, we report the results of simulating the microwave responses of ring resonators using the finite-difference time-domain (FDTD) method [12]. The FDTD method provides a full-wave, time-dependent solution of the Maxwell's equations in 3 D, without making lumped-element approximations of the circuit, or using artifices to model the process of wave propagation. Thus, it enables us to incorporate the real geometrical and material parameters of the object under study into the FDTD simulations.

Misra and Chowdhury have used the FDTD method to simulate microstrip ring resonators [13]; however, their focus is to derive the input impedance (equivalently, the voltage standing-wave ratio) of a concentric microstrip ring antenna. Our objective here is to simulate the scattering parameters of microstrip ring resonators in order to assess the feasibility as well as suitability of the FDTD simulation method for material characterization.

Ring resonators, with and without slits in the coupling zones, of both edge- and side-coupled types, are simulated for the case of infinitely thin strip conductors, as well as for conductors of finite thickness. The effects of magnetic and electric field coupling mechanisms on the resonance are investigated, and the occurrence of resonance peak splitting is demonstrated via the *S*-parameter simulation. Finally, we show that, by fitting the simulation results to the experimental data, we can derive the dielectric properties of the substrate at microwave frequencies.

2. SIMULATION PROCEDURE

Figure 1 depicts the microstrip resonator circuits under study. The design shown in Figure 1(a) models the experimental configuration, and the other three types in Figure 1 are simulated without experimental comparison. The dimensions of the silver ring and the feedline strips deposited on the substrate were 0.25 mm. wide and 0.01 mm thick, and the outside diameter of the ring was 10 mm, the coupling gaps were 0.125 mm wide, and the thickness of the dielectric substrate was 0.625 mm. In the simulation, the dielectric constant for the alumina substrate was initially assumed to be 8.9 [14]. However, a value of 9.3 was found to provide a much better fit between the simulation results and the experimental data.

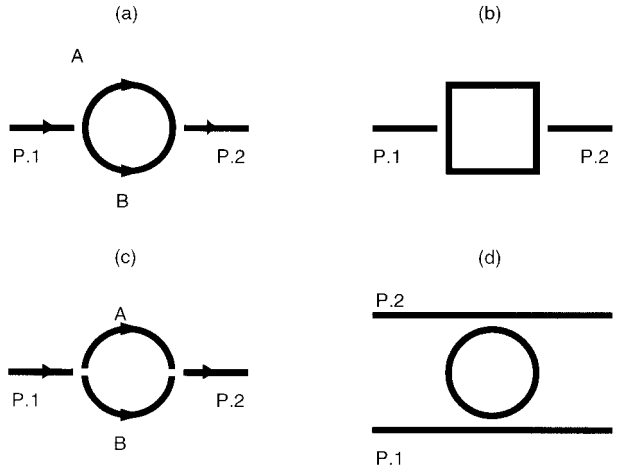

Figure 1 Geometries of ring resonators. (a) Edge-coupled ring resonator. (b) Edge-coupled square resonator. (c) Edge-coupled ring resonator with slits. (d) Side-coupled ring resonator

A square ring design [Fig. 1(b)] was used, as a convenient and first approximation of the circular ring, to assess the feasibility of the FDTD method for microstrip resonator simulations. Staircasing approximations of the circular ring using 20 strips (coarse approximation) and 102 strips (fine approximation) are shown in Figure 2. The latter was found to work sufficiently well for our study, which did not introduce undesirable distortions in the computed resonance characteristics. Therefore, the 102-strip discretization was used in all subsequent simulations of the circuits depicted in Figure 1(a)–(d). The design shown in Figure 1(c) was studied to estimate the effect of the slits introduced in the ring electrode. Figure 1(d) was investigated to determine the coupling effects.

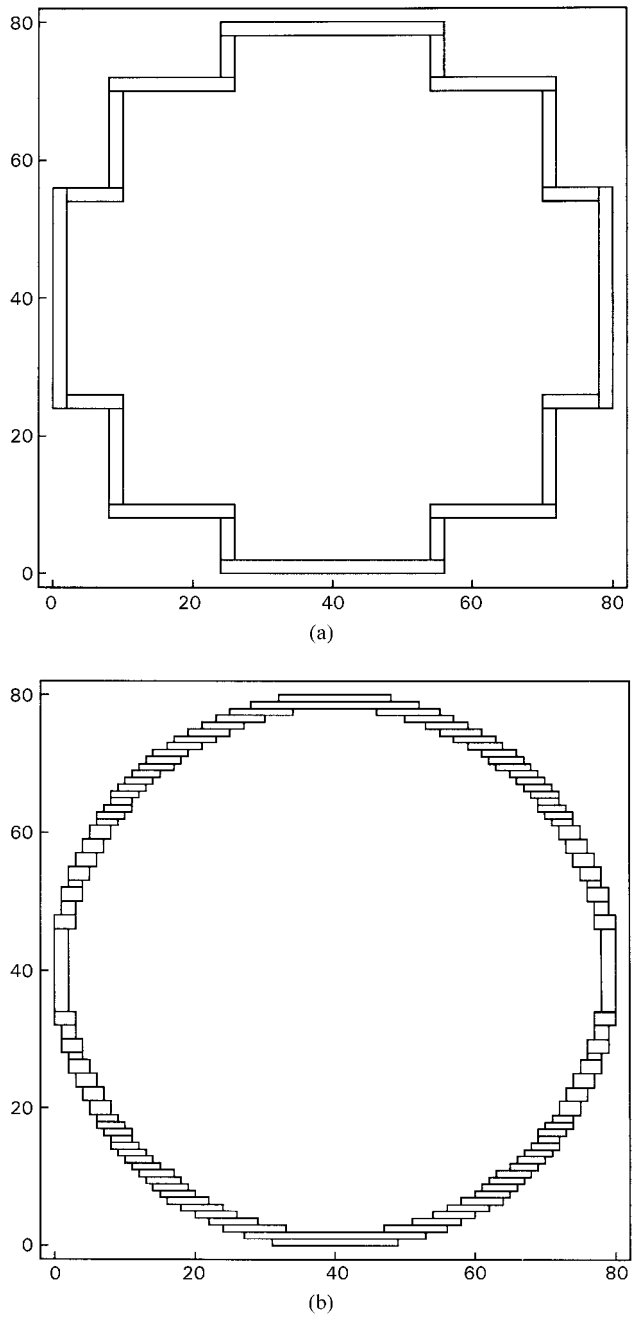

Figure 2 (a) Coarse staircasing approximation of a ring structure using 20 strips. (b) Fine staircasing approximation of a ring structure using 102 strips. Both approximations occupy a grid space of (80 × 80) cells

We have used a computational domain of 120 × 15 × 204 cells, which was chosen to provide a sufficiently large separation between the resonator and the mesh boundary. The cell size was chosen to equal to the width of the coupling gap, i.e., 0.125 mm, and the time step was set to be 0.238322 ps in accordance with the Courant condition [12]. Mur's absorbing boundary conditions [15] were applied at the top, side, and end surfaces of the mesh, while the bottom surface was chosen to be perfectly conducting as the ground plane. A Gaussian-shaped electric field pulse, with its field vector perpendicular to the ground and strip planes, was used to excite the feedline on the left side of the resonator. The bandwidth of the Gaussian-shaped excitation pulse was chosen to be 10 GHz, unless indicated otherwise. The excitation pulse was applied at a point 0.625 mm from the left end of the 7.5 mm long feedline. In order to avoid the introduction of distortions in the incident signal, the distance between the source and the resonator has to be sufficiently large.

From the ratio of the computed transmitted voltage signal to the incident voltage, which was found by removing the ring and extending the microstrip line up to the far absorbing wall, the $S_{21} = V_{tr}(f)/V_{inc}(f)$ parameter was obtained, where $V_{inc}(f)$ and $V_{tr}(f)$ were the Fourier-transformed values of the incident and transmitted voltages, respectively.

Figure 3 illustrates the simulated current transients in the input feedline of a square resonator, and a comparison with the current in an extended microstrip line without the coupled resonator, i.e., the incident current. As seen from the figure, the transient response of the resonant structure exhibits late time oscillations, in contrast to a clean pulse signal that is obtained in an extended microstrip line. Such a long-tailed response can introduce truncation problems in the fast Fourier transform procedure unless a sufficiently long simulation time is used [16].

Figure 4 demonstrates the influence of the width of the simulation time window on the $|S_{21}|$ value calculated from the square resonator design. The two curves plotted correspond to truncation windows of 3000 and 16,384 time steps, respectively. We observed that the calculated resonance frequencies were not influenced strongly by the window width (i.e., by the number of time steps used in the simulation); however, the shape of the $|S_{21}|$ spectrum was found to depend strongly on the number of simulation time steps. We found that the simulation results converged at 16,384 time steps.

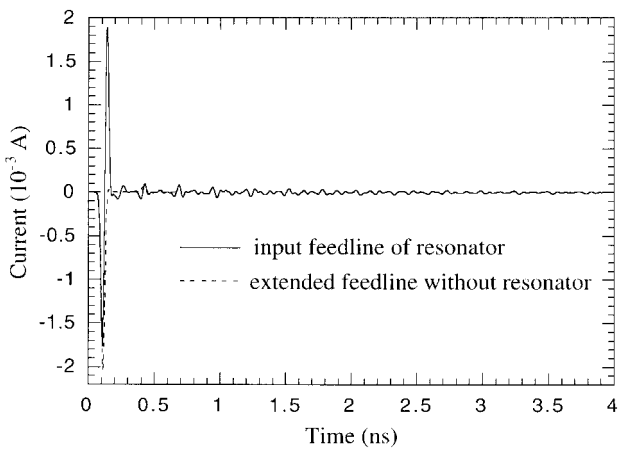

Figure 3 Time dependence of the electric currents in the input feedline of a square resonator (solid curve) and in the extended feedline without resonator (dashed line), respectively

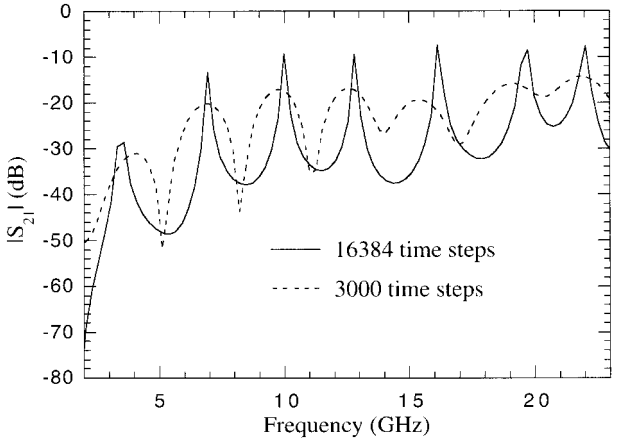

Figure 4 $|S_{21}|$ versus frequency for a square resonator computed by using 3000 time steps (dashed curve) and 16,384 time steps (solid curve), respectively

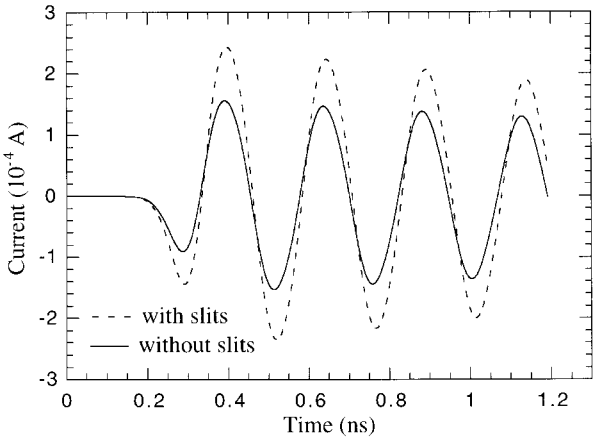

Figure 6 Current versus time at points A and B [Fig. 1(a) and (c)] of ring resonators without slits (solid curve) and with slits (dashed curve), respectively

Figure 5 plots the calculated resonance spectra for the following three resonator designs: 1) square-shaped resonator, 2) coarse staircasing approximation with 20 microstrip sections, and 3) fine staircasing approximation with 102 microstrip sections, as shown in Figures 1(b), 2(a), and 2(b), respectively. It was found that the fine staircasing approximation 3) yielded the best fit with the experimental data.

3. RESULTS

In order to suppress higher order modes, a Gaussian current pulse with a bandwidth of 3 GHz was employed as the excitation signal for the simulation of current distributions in an edge-coupled ring resonator. It was found that the current distribution is symmetric with respect to the feedline axis, and has an approximate form of a half-wavelength standing wave that is established in the two halves of the ring. The observed symmetry of the current flow prompted us to evaluate the effects of slits in the coupling zones of the ring [see Fig. 1(c)]. In order to ensure that a resonator with two slits still has a good coupling, we changed the shape of the feedline at the coupled ends to a T-type. The simulation results in Figure 6 show that the electric currents in the resonator with slits have a higher magnitude and the same flow direction and oscillation frequency as that of the ring resonators without slits. For the resonator with slits, the $|S_{21}|$ spectrum is very similar to that of the ring resonator without slits, although the Q-factor becomes worse (Fig. 7). Gopalakrishnan and Chang [17] have measured the $|S_{21}|$ spectrum for edge-coupled resonators with and without slits, and also did not find any significant change. In other words, these slits, located as shown in Figure 1(c), do not impede the propagation of the electromagnetic waves. It should be noted that the design with slits is very attractive for optoelectronic applications because the slits can be used for optical excitation and electronic tuning or switching.

In order to study the effect of the coupling on the resonator response, we calculated the ring design shown in Figure 1(a) for two metal strips of different thickness. In one case, the strips were infinitely thin—a commonly used approximation in microwave circuit modeling, and for the other case, the thickness of metal strips was set be one cell size. The results of $|S_{21}|$ simulations are given in Figure 8. For the first case, the resonance peaks in the $|S_{21}|$ spectrum showed splitting, with the first peak having the most separation, and the splitting becomes smaller for higher. frequency modes. The peaks corresponding to the magnetic coupling are too

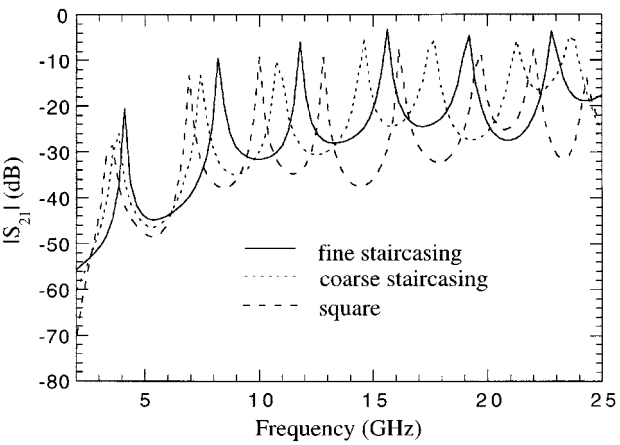

Figure 5 $|S_{21}|$ versus frequency for a square resonator (dashed curve) and a ring resonator computed using coarse (dotted curve) and fine (solid curve) staircasing approximations, respectively

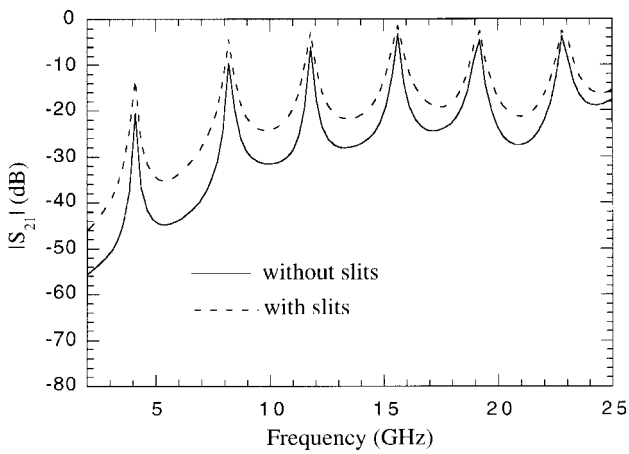

Figure 7 $|S_{21}|$ versus frequency for edge-coupled ring resonators without (solid curve) and with slits (dashed curve), respectively

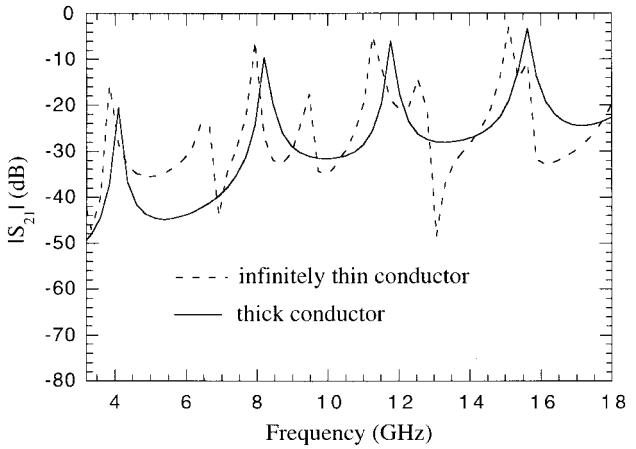

Figure 8 $|S_{21}|$ frequency spectra for ring resonators with infinitely thin strip conductors (dashed curve) and 0.125 mm thick conductors (solid curve), respectively

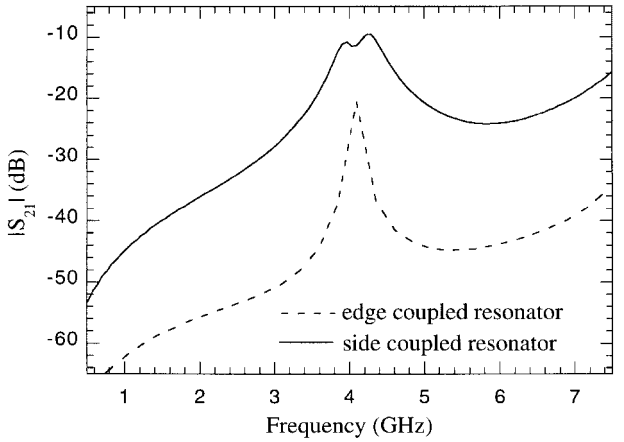

Figure 9 $|S_{21}|$ peaks of the first resonance modes for the edge-coupled (dashed curve) and side-coupled (solid curve) ring resonators, respectively. The thickness of the conducting strips was 0.125 mm

weak to be seen in the case of resonators with thick metal conductors.

The simulation results presented above agree with the experimental observations of Lu and Ferendeci [18, 19] insofar as the first resonance peak splitting is concerned for a side-coupled ring resonator with small coupling gaps. They identified the two sets of peaks with the simultaneous generation of two types of resonant modes by magnetic field coupling and electric field coupling. The values of the coupling coefficients for the two types of modes, as estimated via the transmission-line theory [19], appeared to be comparable to the side-coupled resonators with small coupling gaps.

For the case of the edge-coupled resonator, it appears that the thick conductor mainly provides the electric field coupling owing to the relatively large capacitance of the gaps, while the infinitely thin microstrip approximation leads to a decrease of the electric field coupling, but not the magnetic field coupling. As a result, for the case of infinitely thin metal strips, the coupling becomes similar to that described by Lu and Ferendeci [18, 19], and consequently, leads to the appearance of the two sets of modes.

In order to confirm that our simulations indeed predicted the two types of coupling mechanisms observed by Lu and Ferendeci [19], we also modeled the side-coupled ring resonator as shown in Figure 1(d). The coupling gap and the metal layer thickness were both set to be equal to one cell size for enhancing the electric field coupling. In a side-coupled resonator, however, the magnetic field coupling is expected to be dominant, as observed by Lu and Ferendeci [19], even for gaps as small as 0.05 mm. Figure 9 shows the simulation results of the first resonance mode of $|S_{21}|$ for a side-coupled ring resonator and a comparison with that for an edge-coupled resonator. As expected, the peak of the $|S_{21}|$ spectrum for the side-coupled ring resonator showed splitting, and also had a relatively larger magnitude.

Varying the thickness of the metal layer or the width of the coupling gap offers us two options for changing the strength of the two coupling mechanisms. The splitting of the resonance modes, caused by the enhancement or weakening of one of the coupling mechanisms, may find applications in double-tuned microwave filters.

Next, we turn to the discussion of determining the dielectric constant by fitting the FDTD simulation results to the experimental data. Toward this end, we performed the simulations using the following dielectric constant values: 8.7, 8.9, 9.1, and 9.3. The best fitting to the measured results was achieved when the dielectric constant is equal to 9.3. This value for alumina is 4.5% larger than the value obtained from the tables given in [14]. A comparison of the simulated $|S_{21}|$ spectrum using a dielectric constant value of 9.3 with the experimental data is shown in Figure 10 for a ring resonator with parameters given in Section 2. Good agreement between the simulations and the measurements has been obtained. A most encouraging finding is that we could determine the dielectric constant of the substrate accurately by fitting the FDTD simulation results of ring resonators to experimental data by adjusting the dielectric constant.

It should be mentioned that we did not account for the dielectric loss in the simulations when a pulse excitation (a broadband signal) was used. To account for the dielectric loss, simulations must be performed for each frequency with a frequency-dependent loss factor.

4. CONCLUSIONS

We have used FDTD simulation to study the response of microstrip ring resonators. It was found that the fine staircas-

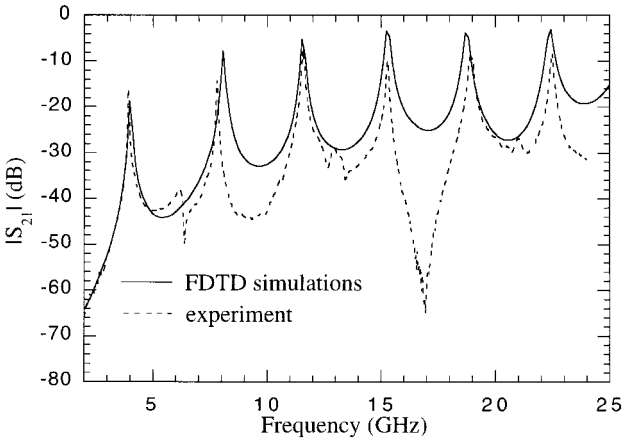

Figure 10 Measured $|S_{21}|$ (f) spectrum for the ring resonator (dashed curve) and $|S_{21}|$ (f) spectrum for the same resonator computed by using the FDTD method (solid curve), respectively

ing approximation of the ring structures was appropriate. Our simulation results showed that slits could be introduced to the ring structures without distorting the frequency response of the resonator. We also found two sets of resonance peaks which can be understood as being due to the existence of two different coupling mechanisms: one through the electric field, and the other through the magnetic field. For infinitely thin conductors, the two sets of peaks could be observed for both edge- and side-coupled ring resonators. It was also demonstrated that one could accurately determine the dielectric constant of the substrate by fitting the FDTD simulation results of a ring resonator response to the experimentally observed S_{21}-parameter spectrum.

ACKNOWLEDGMENT

The authors thank Steven Perini and Michael Lanagan for providing the experimental data of Figure 10.

REFERENCES

1. M.E. Mayercik, Resonant microstrip rings and dielectric material testing, Microwaves (Apr. 1991), 95–102.
2. P.A. Barnard and J.M. Gantray, Measurement of dielectric constant using a microstrip ring resonator, IEEE Trans Microwave Theory Tech 39 (1991), 592–595.
3. H.A. Wheeler, Transmission line properties of parallel strips separated by a dielectric shield, IEEE Trans Microwave Theory Tech MTT-13 (1965), 172–185.
4. M.V. Schneider, Microstrip lines for microwave integrated circuits, Bell Syst Tech J 48 (1969), 1421–1444.
5. E.O. Hammerstad, Equations for microstrip circuit design, Proc European Microwave Conf, Hamburg, Germany, Sept. 1975, pp. 268–272.
6. I.J. Bahl and D.K. Trivedi, A designer's guide to microstrip line, Microwaves (May 1977), 174–181.
7. K. Chang, Microwave ring circuits and antennas, Wiley, New York, 1996.
8. I. Wolff and N. Knoppik, Microstrip ring resonator and dispersion measurements on microstrip lines, Electron Lett 7 (1971), 779–781.
9. R.P. Owens, Curvature effect in microstrip ring resonators, Electron Lett 12, (1976), 356–357.
10. S.G. Pintzos and R. Pregla, A simple method for computing the resonant frequencies of microstrip ring resonators, IEEE Trans Microwave Theory Tech MTT-26 (1978), 809–813.
11. K. Chang, T.S. Martin, F. Wang, and J.L. Klein, On the study of microstrip ring and varactor-tuned ring circuits, IEEE Trans Microwave Theory Tech MTT-35 (1987), 1288–1295.
12. A. Taflove, Computational electrodynamics. The finite-difference time-domain method, Artech House, Boston, MA, London, England, 1995.
13. I.S. Misra and, S.K. Chowdhury, Concentric microstrip ring antenna: Theory and experiment, J Electromag Waves Appl 10 (1996), 439–450.
14. C.A. Harber, Handbook of thick film hybrid microelectronics, McGraw-Hill, New York, 1974.
15. G. Mur, Absorbing boundary conditions for the finite-difference approximation of the time-domain electromagnetic-field equations, IEEE Trans Electromag Compat EMC-23 (1981), 377–382.
16. E.O. Brigham, The fast Fourier transform and its applications, Prentice-Hall, Englewood Cliffs, NJ, 1988.
17. G.K. Gopalakrishnan and K. Chang, Study of slits in microstrip ring resonators for microwave and optoelectronic applications, Microwave Opt Technol Lett 5 (1992), 76–79.
18. S.-L. Lu and A.M. Ferendeci, Coupling modes of a ring resonator side coupled to a microstrip line, Electron Lett 30 (1994), 1013–1015.
19. S.-L. Lu and A.M. Ferendeci, Coupling parameters for a side-coupled ring resonator and a microstrip line, IEEE Trans Microwave Theory Tech 44 (1996), 953–956.

URBAN CHANNEL PROPAGATION MODELING USING THE SHOOTING AND BOUNCING RAY TECHNIQUE

I. Y. Kelly,[1] H. Ling,[1] and W. J. Vogel[1]
[1] Department of Electrical and Computer Engineering
University of Texas at Austin
Austin, Texas 78712-1084

Received 7 October 1999

ABSTRACT: *A study of urban channel characteristics is carried out using the shooting and bouncing ray technique. Propagation characteristics are generated from the simulation, and are compared to measurement results for the downtown area of Austin, TX, at 1.9 GHz. Antenna diversity studies are also carried out using the simulation.* © 2000 John Wiley & Sons, Inc. Microwave Opt Technol Lett 24: 396–399, 2000.

Key words: *propagation; channel modeling; SBR; CPATCH*

1. INTRODUCTION

As the demand for wireless personal communications increases, so does the need for accurate propagation channel models in complex environments. In this work, we carry out a study to characterize the urban propagation channel by using ray tracing. We consider a ray tracer based on the shooting and bouncing ray (SBR) technique [1–3]. The particular scenario addressed has a base-station antenna height below the level of the average urban building, and falls into the microcell category. Propagation characteristics such as slow-fade and fast-fade distributions are examined and compared to measurement results for the downtown area of Austin, TX. The application of the simulation is demonstrated by carrying out spatial and polarization diversity studies.

This paper is organized as follows. In Section 2, we describe the simulation methodology, and present results of the urban channel characteristics simulated using the SBR-based code CPATCH [3] on a CAD model of downtown Austin, TX. In Section 3, the simulation results are compared against measurement data. Both the slow-fade and fast-fade characteristics are examined. In Section 4, an antenna diversity study is carried out using the simulator. Spatial diversity and polarization diversity schemes are investigated to determine the diversity gains of the different scenarios.

2. RAY-TRACING SIMULATION

The SBR-based code CPATCH is used to carry out urban channel simulation. CPATCH is designed for the calculation of antenna coupling in complex environments. It performs these calculations by shooting a dense grid of geometric optic rays from the transmitting antenna, and tracing the rays as they multiply reflect among the surfaces of a CAD description of the environment. After the ray tracing is carried out, the received signal at the receiving antenna is computed by

Contract grant sponsor: Texas Higher Education Coordinating Board under the Texas Advanced Technology Program